mathematics

MDPI

Article

Transient Response Enhancement of PMD Battery Charger Using Rule-Based Fuzzy Logic Control

Gijeong Yoon [1] and Yeongsu Bak [2,*]

[1] Department of Electronic and Electrical Engineering, Keimyung University, Daegu 42601, Republic of Korea; gjyoon@kmu.kr
[2] Department of Electrical Engineering, Keimyung University, Daegu 42601, Republic of Korea
* Correspondence: ysbak@kmu.ac.kr

Abstract

This paper proposes a transient response enhancement of a personal mobility device (PMD) battery charger using a rule-based fuzzy logic control (RBFLC) method. PMD encompasses various applications, including electric kickboards, electric scooters, and electric wheelchairs. The rated battery voltage required for each device is different; additionally, the PMD battery charger must be accurate and have a fast transient response. However, when the gain is significantly increased in the conventional proportional-integral (PI) control method to enhance the transient response, the battery charger output voltage exhibits oscillatory behavior and becomes unstable. Therefore, in this paper, the RBFLC method is proposed to improve the transient response performance of the battery charger without oscillation and instability of the output voltage. The proposed RBFLC method is verified through simulation and experimental results.

Keywords: battery charger; personal mobility device; future mobility; rule-based fuzzy logic control; transient response

MSC: 93C42; 94D05

1. Introduction

AS eco-friendly policies aimed at reducing environmental pollution, fossil fuel depletion, and greenhouse gas emissions are being strengthened globally, the demand for personal mobility devices (PMDs) is rapidly increasing. The PMD includes electric kickboards, electric scooters, and electric wheelchairs powered by electricity. It offers the advantages of being lightweight and compact compared to internal combustion engine vehicles [1–3].

To charge the battery of PMD, different rated voltages are required for each device. For example, electric kickboards and electric scooters require 36 V, whereas electric wheelchairs require 24 V. Therefore, the PMD battery charger must be able to regulate the output voltage over a wide range. However, since conventional PMD battery charger is designed for a single fixed voltage, it results in compatibility issues and user inconvenience. For these reasons, growing interest is being shown in PMD battery charger technologies that ensure stable operation while regulating the output voltage over a wide range [4–7].

The PMD battery charger that regulates the output voltage over a wide range employs using various converter topologies such as buck converter, boost converter, buck–boost converter, flyback converter, and resonant converter [8–11]. In this paper, a three-stage

Check for updates

Academic Editors: Soo-Ho Jo, Haichao An and Jaehun Lee

Received: 12 January 2026
Revised: 5 February 2026
Accepted: 6 February 2026
Published: 7 February 2026

Copyright: © 2026 by the authors. Licensee MDPI, Basel, Switzerland. This article is an open access article distributed under the terms and conditions of the Creative Commons Attribution (CC BY) license.

power conversion structure consisting of a power factor correction (PFC) boost converter, a half-bridge LLC resonant converter, and a buck converter is employed. It offers simplified voltage regulation, enhanced efficiency, and stable operation over a wide voltage range, making it highly suitable for a PMD battery charger. In the first stage, the PFC boost converter ensures a high power factor and low total harmonic distortion (THD) by regulating the input current to track the phase of the input voltage and maintaining a constant output voltage. In the second stage, an LLC resonant converter is employed, enabling a high power density through high-frequency operation and achieving high efficiency through soft switching and resonance characteristics. Finally, in the third stage, a buck converter regulates the output voltage to match the rated battery voltage of PMD [12–15].

In general, a proportional-integral (PI) controller is used to regulate the buck converter output voltage of the battery charger because of its simplicity and ease of implementation. The gain of the PI controller affects control performance [16,17]. Reducing the proportional gain decreases the responsiveness of the PMD battery charger due to an overdamped response. With increasing the proportional gain enhances responsiveness, however, comes overshooting and oscillations due to an underdamped response. These disadvantages reduce the stability and lifespan of PMD battery charger, which reduces their commercial viability [18,19]. Therefore, to reduce the instability of the PMD battery charger caused by oscillations, a different control strategy is needed.

To remove the drawbacks of the PI controller, a fuzzy logic control (FLC) method, which is a form of artificial intelligence-based control, can be employed. The FLC method transforms discrete control rules into continuous control values, making it easy to express control logic in linguistic terms. The FLC method generally consists of fuzzification, fuzzy inference, defuzzification. In particular, in the fuzzification as the process of converting the input variables into the value required for fuzzy inference, a crisp set is used in groups with clear boundaries, and a fuzzy set is used in groups with ambiguous boundaries [20,21]. The crisp set has a binary characteristic where an element either fully belongs to the set or does not belong at all, providing a clear true or false decision. However, when an element has ambiguous characteristics, the binary structure of a crisp set results in discontinuous control operation, which becomes a disadvantage in achieving precise control. Therefore, the fuzzy set is generally used instead of the crisp set to achieve more precise control. The fuzzy set is defined using a membership function, which is used to numerically express the degree to which an element belongs to the set [22,23].

As a result, using the FLC method, the nonlinear characteristics of the control system and the uncertainties between inputs and outputs can be expressed in linguistic terms. Therefore, it provides strong robustness against load variations, external disturbances, and noise. Furthermore, it offers the advantage of flexibly responding to errors based only on the input–output relationship, even when it is difficult to mathematically approximate the system or when the system shows nonlinear characteristics [24–28]. However, the conventional FLC method can reduce the accuracy in a complex control system due to its single input.

Therefore, in this paper, a rule-based fuzzy logic control (RBFLC) method for transient response enhancement of the PMD battery charger is proposed. The proposed RBFLC method uses two input variables: the output voltage error and the change of the output voltage error of the PMD battery charger. It operates based on a rule-based table and can consider various conditions, enabling precise control of the PMD battery charger. For these reasons, the proposed method can enhance the transient response compared to the PI controller, in addition to achieving fast responsiveness without overshoot. The effectiveness of the proposed method is validated through simulation and experimental results.

2. PMD Battery Charger

2.1. Structure of PMD Battery Charger

Figure 1 presents the topology of the power conversion stages of the PMD battery charger. It consists of a three-stage power conversion structure consisting of a PFC boost converter, a half-bridge LLC resonant converter, and a buck converter. It enables the PMD battery charger to efficiently and stably regulate the output voltage according to the rated voltages of various PMD.

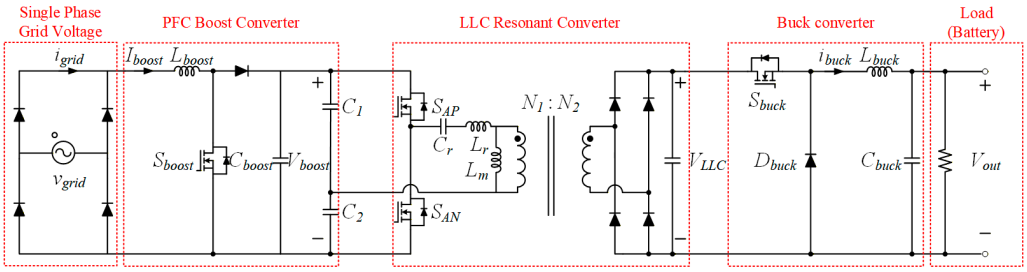


Figure 1. Topology of the power conversion stages of the PMD battery charger.

First, a single-phase AC grid voltage of 220 V_{rms}/60 Hz is supplied to the input of a diode rectifier, which converts the AC voltage into a DC voltage. The transformed DC voltage is supplied to the input of the PFC boost converter, which is the first stage of the three-stage converter. The PFC boost converter steps up the input voltage to a higher level. It also regulates the input current phase to be aligned with the input voltage phase. Therefore, the power factor of the output power is improved, and the THD of the output voltage and current is reduced. The second stage employs the half-bridge LLC resonant converter, which steps down the boosted voltage using high-frequency switching and a resonant circuit. It enables soft switching, improving power density and efficiency. Additionally, the transformer used in this stage provides galvanic isolation between the input and the output, ensuring electrical safety. Finally, the output stage employs the buck converter that drives the switching device based on the duty cycle. It regulates the output voltage of the PMD battery charger based on the rated voltage of the PMD. In this paper, a resistive load is used instead of actual PMD batteries. Using the three-stage power conversion topology, the PMD battery charger offers a high power factor, low THD, electrical stability, and the ability to regulate the output voltage over a wide range.

2.2. Operating Principle of PMD Battery Charger

Figure 2 presents the operating principle of the buck converter. The output voltage of the buck converter is controlled by the ON and OFF operation of the switch (S_{buck}). Mode 1 occurs when S_{buck} is ON, and the diode is OFF. In this mode, the inductor voltage (V_L) is given by the difference between the input voltage (V_{LLC}) and the output voltage (V_{out}), and the inductor current (i_{buck}) increases. Mode 2 occurs when S_{buck} is OFF, and the diode is ON. In this mode, V_L is $-V_{out}$, and i_{buck} decreases. Over one switching period T, V_L is expressed as in (1).

$$V_L = (V_{LLC} - V_{out})d_{buck}T + (-V_{out})(1 - d_{buck})T, \tag{1}$$

where d_{buck} is the duty ratio.

At steady state, due to volt-second balance, V_L is zero over one switching period, and d_{buck} is obtained as in (2).

$$d_{buck} = \frac{V_{out}}{V_{LLC}}. \tag{2}$$

The d_{buck} is compared with a carrier signal to generate the PWM gate signal for S_{buck}.

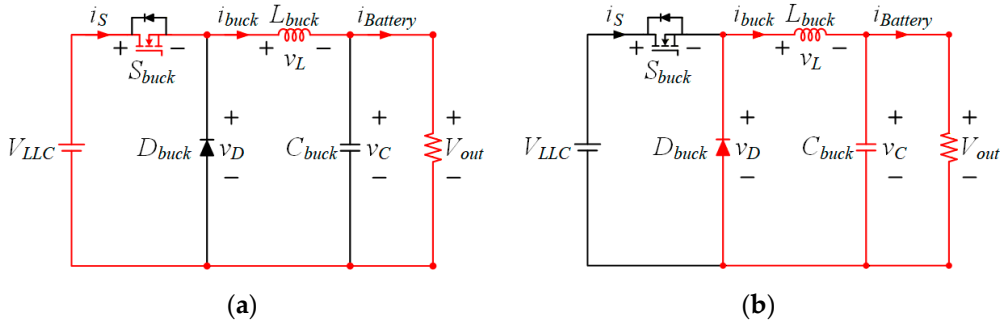


Figure 2. Operating principle of the buck converter: (**a**) Mode 1; (**b**) Mode 2.

3. Proposed Rule-Based Fuzzy Logic Control

This paper proposes the RBFLC method to enhance the transient response of the PMD battery charger. The proposed RBFLC method uses two input variables and employs a more detailed rule-based table than the conventional FLC method, offering advantages such as improved control accuracy, enhanced transient response, and suppression of overshoot. Figure 3 presents the control block diagram of the RBFLC method. The input variables of the RBFLC are output voltage error (V_{err}) and change of output voltage error (ΔV_{err}). The V_{err} is calculated from the error between the reference output voltage (V^*_{out}) and V_{out} of the PMD battery charger, as in (3).

$$V_{err} = V^*_{out} - V_{out}. \tag{3}$$

The ΔV_{err} is calculated from the error between V_{err} at the current sampling period (k) and the previous sampling period ($k-1$) as in (4).

$$\Delta V_{err}(k) = V_{err}(k) - V_{err}(k-1). \tag{4}$$

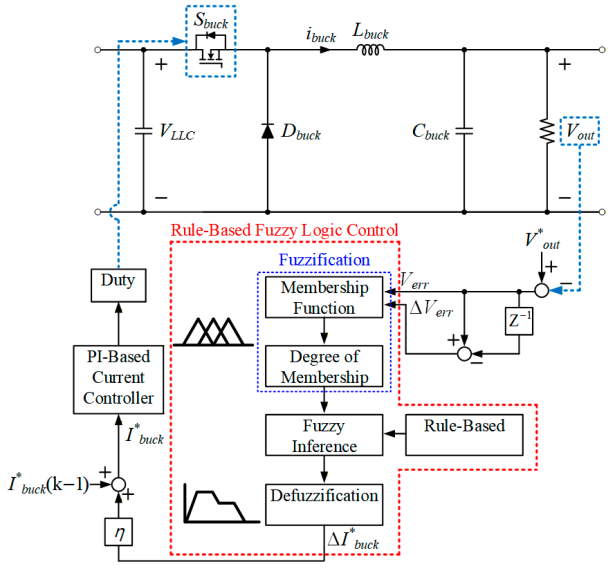


Figure 3. Control block diagram of the RBFLC method.

The V_{err} and ΔV_{err} are used as input to the RBFLC, which consists of fuzzification, fuzzy inference, and defuzzification. Through the RBFLC, V_{out} can be controlled to V^*_{out}, as a result, the change of reference current of the buck converter (ΔI^*_{buck}) can be obtained. In addition, a reference current of the buck converter (I^*_{buck}) is calculated by ΔI^*_{buck} and a

reference current in a previous sampling period ($I^*_{buck}(k-1)$). Finally, by using the PI-based current controller, I_{buck} can be controlled to I^*_{buck}.

3.1. Fuzzification

Fuzzification is the process of converting V_{err} and ΔV_{err} of the PMD battery charger into the degree of membership (DOM) using a defined membership function. The DOM expressed between 0 and 1 represents the degree of belonging in the fuzzy set, and it is used as an input of the fuzzy interference. Due to the membership function in the RBFLC method affecting the control performance of the PMD battery charger, the range of V_{err} and ΔV_{err} should be considered when calculating the DOM.

The membership function includes various types, such as singleton, Gaussian, and triangular. A singleton type assigns a membership value of 1 to a specific value, and 0 to all others. It simplifies computations in the fuzzy inference stage. However, a singleton type lacks the ability to reduce the noise of the input value. The Gaussian type employs an exponential function and offers noise reduction but increases mathematical complexity. The triangular membership function reduces noise in the input value and simplifies computations in the fuzzy inference stage when IF-THEN rules are applied. Figure 4 presents the triangular membership function, and it is expressed as in (5).

$$u_{tr}(x) = \frac{(x-r)}{(r-p)} + 1(p < x \le r),\ u_{tr}(x) = -\frac{(x-r)}{(q-r)} + 1(r < x \le q), \tag{5}$$

where p is the x-value where the function begins rising from zero, r is the x-value where the function reaches peak, q is the x-value where the function finishes decreasing back to zero.

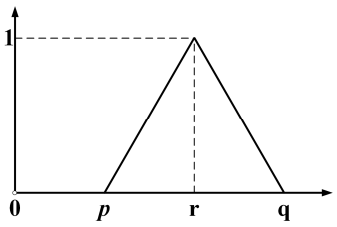
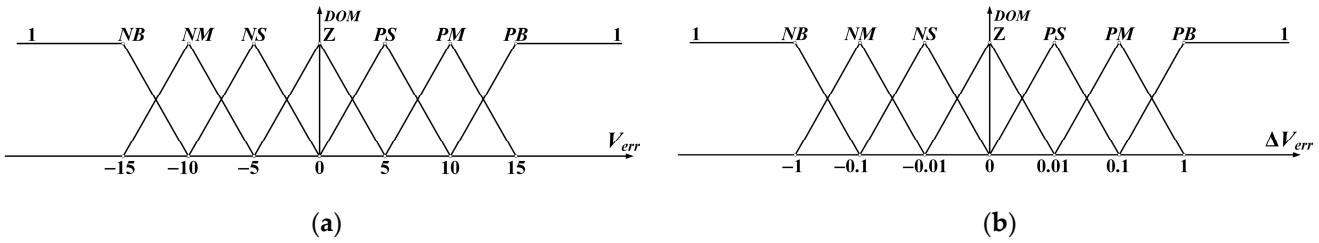


Figure 4. Triangular membership function.

Figure 5 presents the membership function of V_{err} and ΔV_{err}. In the membership function of V_{err} and ΔV_{err} as shown in Figure 5a,b, the range of V_{err} as the x-value is set to -15, -10, -5, 0, 5, 10, 15, and the range of ΔV_{err} is set to -1, -0.1, -0.01, 0, 0.01, 0.1, 1, considering the instantaneous variation of the input variables of the RBFLC. In addition, the peak value of the membership function is assigned to the linguistic terms, which are positive very big (PVB), positive big (PB), positive medium (PM), positive small (PS), negative very big (NVB), negative big (NB), negative medium (NM), negative small (NS), zero (Z).



(**a**) (**b**)

Figure 5. Membership function of (**a**) V_{err}; (**b**) ΔV_{err}.

Figure 6 presents the calculation process of the DOM using the membership function when V_{err} is 7, and ΔV_{err} is -0.08. Firstly, when V_{err} is 7, DOM belongs to two linguistic terms, such as PS and PM. Therefore, DOM of PS and DOM of PM are calculated as in (6) by using the triangular membership function as in (5).

$$\begin{aligned} PS_{Verr}(7) &= -\frac{(x-r)}{(q-r)} + 1 = -\frac{(7-5)}{(10-5)} + 1 = 0.6, \\ PM_{Verr}(7) &= \frac{(x-r)}{(r-p)} + 1 = \frac{(7-10)}{(10-5)} + 1 = 0.4. \end{aligned} \tag{6}$$

Secondly, when ΔV_{err} is -0.08, DOM belongs to two linguistic terms, such as NM and NS. Therefore, DOM of NM and DOM of NS are calculated as in (7) by using the triangular membership function as in (5).

$$\begin{aligned} NM_{\Delta Verr}(-0.08) &= -\frac{(x-r)}{(q-r)} + 1 = -\frac{((-0.08)-(-0.1))}{((-0.01)-(-0.1))} + 1 = 0.78, \\ NS_{\Delta Verr}(-0.08) &= \frac{(x-r)}{(r-p)} + 1 = \frac{((-0.08)-(-0.01))}{((-0.01)-(-0.1))} + 1 = 0.22. \end{aligned} \tag{7}$$

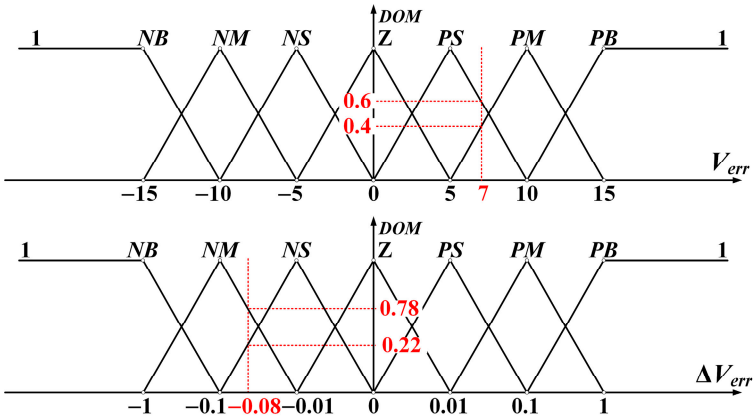


Figure 6. Calculation process of DOM using the membership function when V_{err} is 7 and ΔV_{err} is -0.08.

3.2. Fuzzy Inference

Fuzzy inference is the process of determining a fuzzy conclusion from input variables converted into fuzzy values using fuzzy rules. Linguistic terms belonging to the DOM of V_{err} and ΔV_{err} are used in IF-THEN rules to determine the fuzzy conclusion ΔI^*_{buck}. Figure 7 presents the membership function of ΔI^*_{buck}. The range of ΔII^*_{buck} as the x-value is set to -1, -0.75, -0.5, -0.25, 0, 0.25, 0.5, 0.75, and 1. The IF-THEN rules using the fuzzy rule-based table are as in (8).

$$\textit{If } x \textit{ is } A \textit{ and } y \textit{ is } B \textit{ then } z \textit{ is } C, \tag{8}$$

where x and y are input variables of RBFLC, and z is the output variable of RBFLC. In the battery charger for PMD, x, y and z represent V_{err}, ΔV_{err} and ΔI^*_{buck}; additionally, A, B, and C represent the linguistic terms for V_{err}, ΔV_{err}, and ΔI^*_{buck}. When the IF statement is determined by the linguistic terms (A, B) of V_{err} and ΔV_{err}, the THEN statement assigns the corresponding linguistic term (C) to ΔI^*_{buck}. To improve the transient response of the RBFLC, the fuzzy rule-based table should consist of various rules. If there are more rules, the input variables can be divided in more detail; therefore, the control accuracy of the RBFLC becomes more accurate. In this paper, the fuzzy rule-based table consists of 49 fuzzy control rules listed in Table 1.

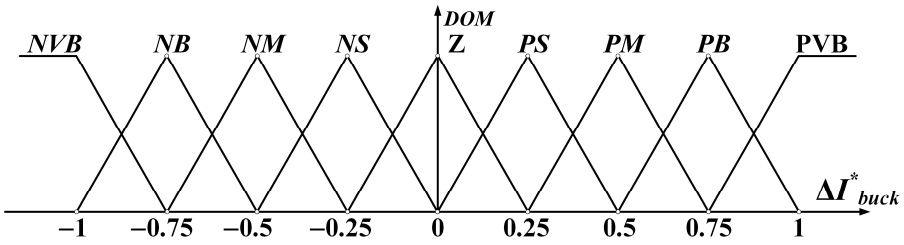


Figure 7. Membership function of ΔI^*_{buck}.

Table 1. Fuzzy rule-based table.

V_{err} \ ΔV_{err}	NB	NM	NS	Z	PS	PM	PB
NB	NVB	NVB	NB	NB	NS	NS	Z
NM	NB	NB	NM	NM	NS	Z	PS
NS	NB	NM	NS	NS	Z	PS	PM
Z	NB	NM	NS	Z	PS	PM	PB
PS	NM	NS	Z	PS	PM	PM	PB
PM	NS	Z	PS	PM	PM	PB	PB
PB	Z	PS	PM	PB	PB	PVB	PVB

Figure 8 presents the fuzzy inference process, where the IF-THEN rules determine the fuzzy conclusion of ΔI^*_{buck}. In the case where V_{err} is 7 and ΔV_{err} err is -0.08, the linguistic terms of V_{err} as PS and PM and ΔV_{err} as NM and NS, as shown in Figure 5. As a result, the fuzzy rules can be defined using Table 1 and the IF-THEN rules are expressed as in (9).

$$\begin{aligned} &\textit{If } V_{err} \textit{ is PS and } \Delta V_{err} \textit{ is NM then } \Delta I^*_{buck} \textit{ is NS},\\ &\textit{If } V_{err} \textit{ is PS and } \Delta V_{err} \textit{ is NS then } \Delta I^*_{buck} \textit{ is Z},\\ &\textit{If } V_{err} \textit{ is PM and } \Delta V_{err} \textit{ is NM then } \Delta I^*_{buck} \textit{ is Z},\\ &\textit{If } V_{err} \textit{ is PM and } \Delta V_{err} \textit{ is NS then } \Delta I^*_{buck} \textit{ is PS}. \end{aligned} \tag{9}$$

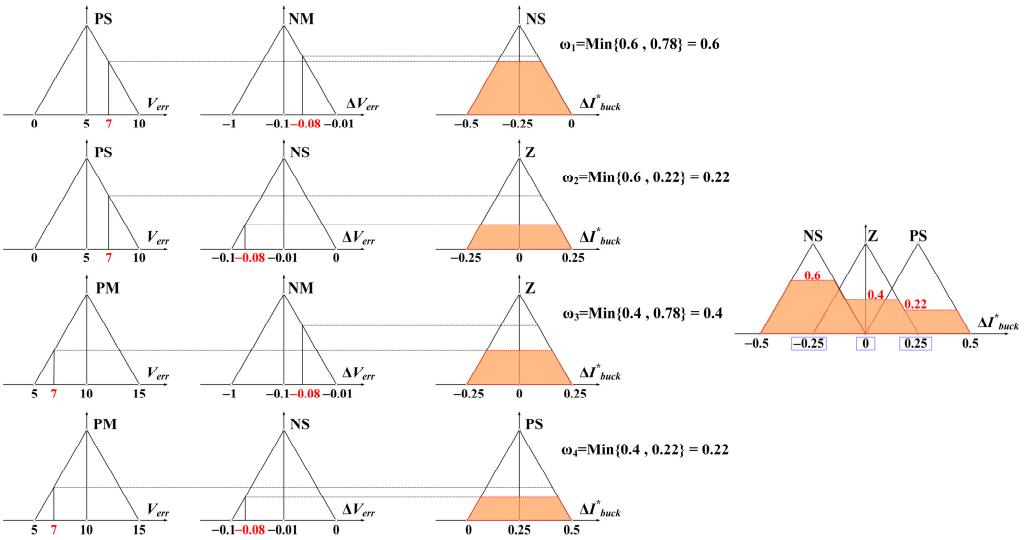


Figure 8. Fuzzy inference process.

After applying the IF-THEN rules, the Min-Max inference method of Mamdani should be applied as shown in Figure 7. The result of the Min-Max inference method is represented

by the weight ω_i, which is calculated as the minimum value of the DOM of V_{err} and ΔV_{err} as in (10).

$$\omega_i = \text{Min}\{\text{DOM}(V_{err}), \text{DOM}(\Delta V_{err})\}, \tag{10}$$

where i is the number of each IF-THEN rule. As with the fuzzy rules, weights are defined as in (11), and the weights are employed in the defuzzification stage.

$$\begin{aligned} \omega_1 &= \text{Min}\{0.6, 0.78\} = 0.6, \\ \omega_2 &= \text{Min}\{0.6, 0.22\} = 0.22, \\ \omega_3 &= \text{Min}\{0.4, 0.78\} = 0.4, \\ \omega_4 &= \text{Min}\{0.4, 0.22\} = 0.22. \end{aligned} \tag{11}$$

3.3. Defuzzification

Defuzzification is the process of converting the fuzzy conclusion into a numerical value, and it is the final stage of the RBFLC. Various defuzzification methods exist, such as the center of gravity, maximum method, and center of average. The center of gravity provides high control accuracy; however, it requires complex calculations and longer processing time. The maximum method entails a simple calculation process; however, it lacks control accuracy. Therefore, in this paper, the center of average method is employed for its computational simplicity and high control accuracy as in (12).

$$\Delta I^*_{buck} = \frac{\sum_{i=1}^{n} \omega_i C_i}{\sum_{i=1}^{n} \omega_i}, \tag{12}$$

where C_i represents the output intensity, which indicates the degree to which the weight is effects in the output of RBFLC. When the linguistic rule of ΔI^*_{buck} is NS, Z, and PS, the C_i is set to -0.25, 0, and 0.25, respectively. Therefore, the ΔI^*_{buck} is calculated as in (13) by using the center of average method as in (12), and it is the output of the RBFLC.

$$\Delta I^*_{buck} = \frac{\omega_1 C_1 + \omega_2 C_2 + \omega_3 C_3 + \omega_4 C_4}{\omega_1 + \omega_2 + \omega_3 + \omega_4} = \frac{0.6 \times (-0.25) + 0.22 \times 0 + 0.4 \times 0 + 0.22 \times 0.25}{0.6 + 0.22 + 0.4 + 0.22}. \tag{13}$$

Finally, the ΔI^*_{buck} is added to the $I^*_{buck}(k-1)$ to calculate the I^*_{buck} as in (14).

$$I^*_{buck}(k) = I^*_{buck}(k-1) + \eta \cdot \Delta I^*_{buck}, \tag{14}$$

where η represents the gain of the RBFLC. In addition, the I^*_{buck} is used as the input of the PI-based current controller.

3.4. Stability Analysis of the RBFLC

The transfer function of the proposed RBFLC-based PMD battery charger is required for stability analysis. However, it is difficult to derive an accurate transfer function that reflects the nonlinear characteristics of the RBFLC. Therefore, in this paper, the PMD battery charger is considered as a black-box model and analyzed based on the discrete input and output data. To analyze the discrete data, the least square parameter estimation algorithm was employed, and the transfer function of the RBFLC-based PMD battery charger was constructed based on the estimated parameters. It is transformed into a continuous transfer function by applying the zero-order-hold method [29] and represented as in (15).

$$G(S) = \frac{b_1 s^3 + b_2 s^2 + b_3 s^1 + b_4}{s^4 + a_1 s^3 + a_2 s^2 + a_4} \cdot \left(K_{pv} + \frac{K_{iv}}{s}\right) \cdot \left(K_{pc} + \frac{K_{ic}}{s}\right), \tag{15}$$

where k_{pv} and k_{iv} represent the proportional and integral gains of the RBFLC-based voltage controller, and k_{pc} and k_{ic} indicate the proportional and integral gains of the PI-based current controller. The transfer function G(s) of the RBFLC is represented as in (16).

$$G(S) = \frac{5.512e^5s^3+6.198e^{10}s^2+2.382e^{17}s^1+4.321e^{21}}{s^4+4.756e^5s^3+1.528e^{11}s^2+4.453e^5s^1+1.06s^{19}} \cdot \left(0.997198 + \frac{2843}{s}\right) \cdot \left(0.00679253 + \frac{2.72}{s}\right), \quad (16)$$

where k_{pv}, k_{iv}, k_{pc} and k_{ic} are set to 0.997198, 2843, 0.13585060, and 54.40. In addition, the stability of the proposed RBFLC can be analyzed using the transfer function G(s) through the Bode diagram and the poles and zeros on the complex plane.

Figure 9 shows the Bode diagram of the transfer function G(s). In Figure 8, the gain crossover frequency is about 10,000 rad/s, and the gain margin is 12 dB. Phase crossover frequency is about 100 rad/s, and phase margin is 49°. Therefore, the stability of the RBFLC for the PMD battery charger is confirmed through the Bode diagram analysis.

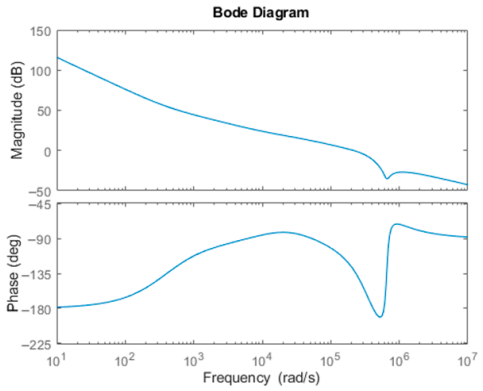


Figure 9. Bode diagram of the transfer function G(s).

Figure 10 shows the pole-zero map of the transfer function G(s) on the complex plane. In Figure 10, all poles are located in the left half plane (LHP). Therefore, based on the stability analysis using the pole-zero map, the stability of the RBFLC-based PMD battery charger can be confirmed.

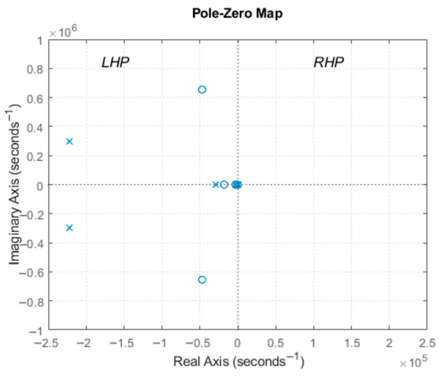


Figure 10. Pole-zero map of the transfer function G(s) on complex plane.

4. Simulation Results

To validate the proposed RBFLC method for the PMD battery charger, simulations were conducted using the PSIM 2020 version and MATLAB 2024 version simulation software. The parameters used in the simulations are shown in Table 2. When a battery is used as the load, the battery characteristics change with operating conditions. Therefore, a resistor load was employed to provide a stable and repeatable operating condition, allowing a

consistent comparison between the two controllers. The load resistance was set to 5 Ω. In this paper, the 36 V electric kickboard is selected as the representative PMD application.

Table 2. Simulation parameter.

Parameters	Value	Unit	Parameters	Value	Unit
P_{rated}	1	kW	v_{grid}	220	V_{rms}
L_{boost}	500	μH	f_{grid}	60	Hz
C_r	2	μF	C_{boost}	1000	μF
L_m	73	μH	L_r	10.4	μH
L_{buck}	500	mH	N_1:N_2	14:7	-
R_{Load}	5	Ω	C_{buck}	1000	μF
T_{samp}	12.5	μs	-	-	-

Figure 11 presents various simulation results of the PMD battery charger. Figure 11a,b presents the 220 V_{rms}/60 Hz single-phase grid voltage (v_g) and current (i_g), which are rectified through the diode rectifier. The PFC boost converter aligns the phase of v_g and i_g to correct the power factor. Figure 11c presents the output voltage (V_{boost}) of the PFC boost converter, which regulates the rectified voltage to 400 V. Figure 11d presents the output voltage (V_{LLC}) of the half-bridge LLC resonant converter, which stepped down the V_{boost} to 100 V according to the turns ratio of the transformer. Figure 11e,f presents the output current (I_{out}) and voltage (V_{out}) of the battery charger for PMD, which are regulated to 7.2 A and 36 V.

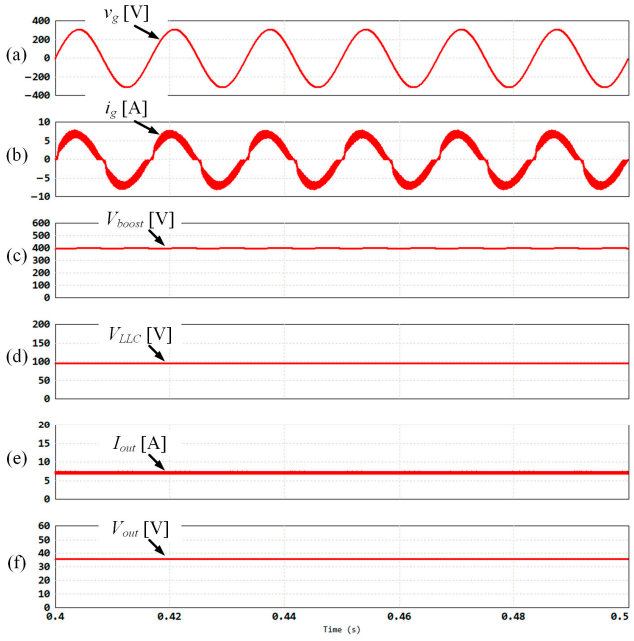
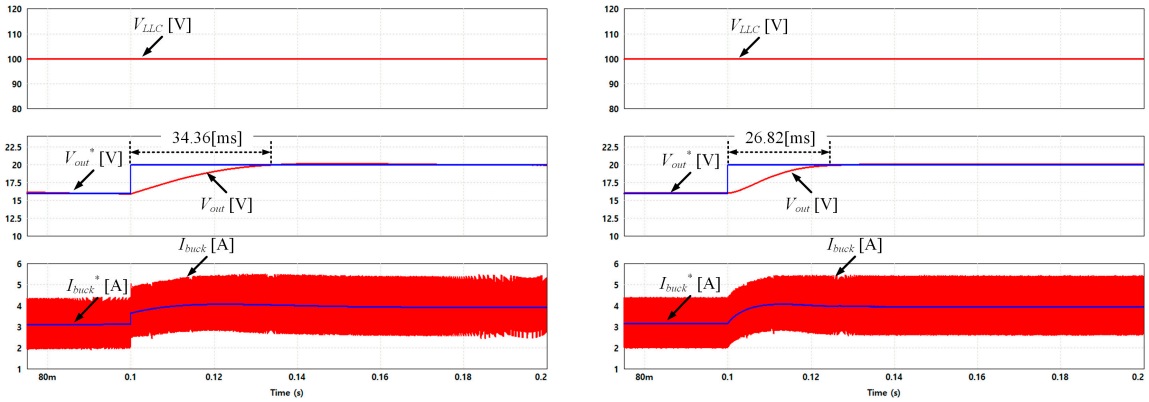


Figure 11. Various simulation results of the PMD battery charger: (**a**) Voltage of the single-phase grid; (**b**) current of the single-phase grid; (**c**) PFC boost converter output voltage; (**d**) half-bridge LLC resonant converter output voltage; (**e**) battery charger output current; (**f**) battery charger output voltage.

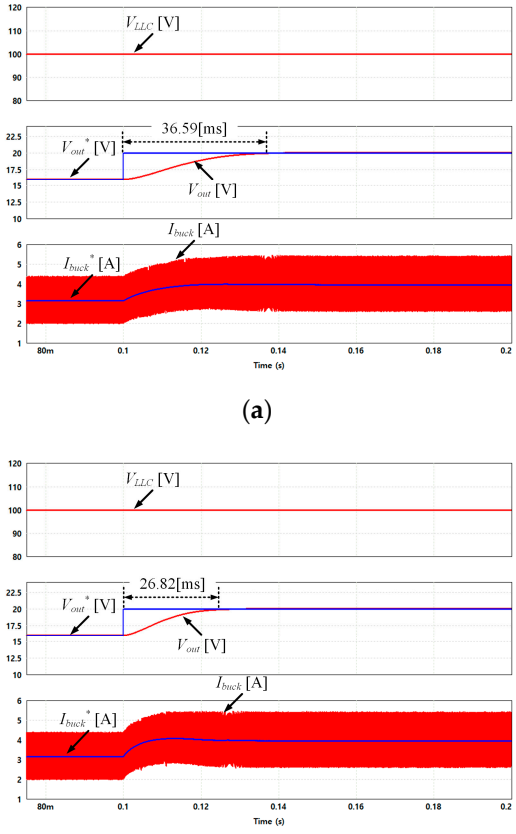
Figure 12 presents the simulation results of transient state responses of the battery charger, comparing the PI controller and the proposed RBFLC method. The V_{LLC} is controlled to 100 V, and the V^*_{out} is changed from 16 V to 20 V at 0.1 s. Figure 12a presents simulation results using the PI controller, with V_{out} to reach V^*_{out} in 36.59 ms. Adjusting the gain of the PI controller can improve responsiveness, which may cause overshoot. Figure 12b presents simulation results using the proposed RBFLC method, with V_{out} to reach V^*_{out} in 26.82 ms. Compared to the PI controller, the proposed RBFLC method improves responsiveness by approximately 26.7%.



(**a**) (**b**)

Figure 12. Simulation results of transient state responses: (**a**) PI controller; (**b**) proposed RBFLC.

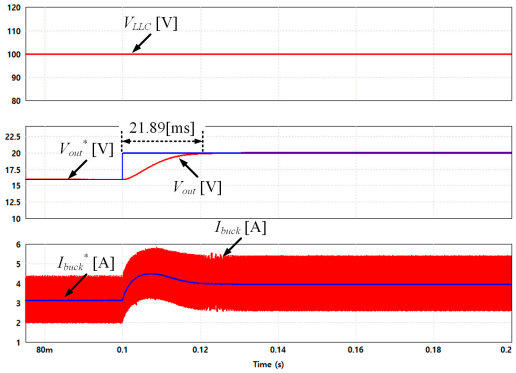
Figure 13 presents the simulation results of the proposed RBFLC method for different values of η. Increasing the value of η improves responsiveness. Figure 13a presents the simulation results when η is set to 0.01, with V_{out} to reach V^*_{out} in 36.59 ms. Figure 13b presents the simulation results when η is set to 0.05, with V_{out} to reach V^*_{out} in 26.82 ms. Figure 13c presents the simulation results when η is set to 0.1, with V_{out} to reach V^*_{out} in 21.89 ms. Considering the change of I^*_{buck} during one sampling period, setting η over 0.1 increases the impact of the compensated ΔI^*_{buck}; therefore, the η value of 0.05 is suitable for the proposed RBFLC method.



(**a**)

(**b**)

Figure 13. *Cont.*



(**c**)

Figure 13. Simulation results of the proposed RBFLC method for different values of η: (**a**) η is 0.01; (**b**) η is 0.05; (**c**) η is 0.1.

5. Experimental Results

Figure 14 presents the experimental setup consisting of the PMD battery charger, a 5 Ω load resistor, and an AC power supply. The experimental results validate the effectiveness of the proposed RBFLC method. The AC power supply provides a single-phase voltage of 220 V_{rms}/60 Hz. The experimental configuration of the PMD battery charger includes the diode rectifier, the PFC boost converter, the half-bridge LLC resonant converter, and the buck converter. The PMD battery charger operates with the AC power supply as input and conducting step up, step down, and compensation through each converter. These operations are controlled by a TMS320F28335 digital signal processor. An independent SMPS powers the TMS320F28335, the current and voltage sensors, and the cooling system. The parameters used in the experiment are the same as those in Table 2.

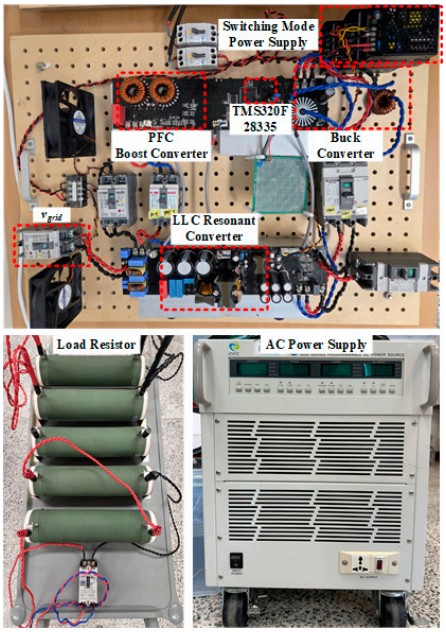


Figure 14. Experimental setup.

Figure 15 presents various experimental results of the PMD battery charger. v_g and i_g are used as the input to the diode rectifier, which rectifies alternating power into direct power. The rectified power is used as the input to the PFC boost converter, which aligns the phase of v_g and i_g to correct the power factor. In addition, the PFC boost converter steps up the rectified voltage to 400 V, which is V_{boost}. The V_{boost} is used as the input to the

half-bridge LLC resonant converter, which stepped down the V_{boost} to 100 V according to the turns ratio of the transformer, which is V_{LLC}. Finally, V_{LLC} is used as the input to the PMD battery charger, which regulates the I_{out} and V_{out} to 7.2 A and 36 V.

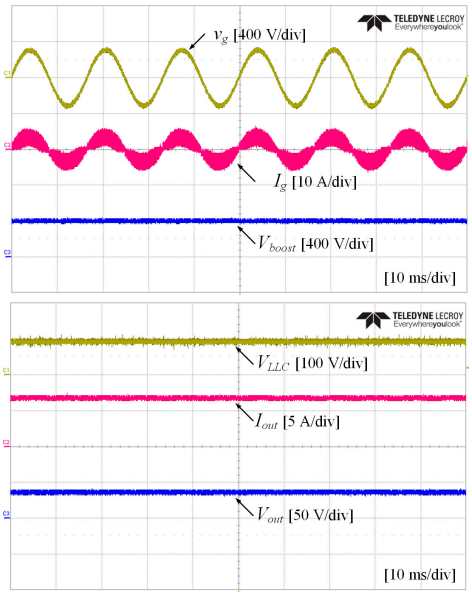


Figure 15. Various experimental results of the PMD battery charger.

Figure 16 presents experimental results of power factor and efficiency analysis in the PMD battery charger. By controlling the power factor of the single-phase input through the PFC boost converter, the power factor reached approximately 0.94, and efficiency was measured at about 90.9%.

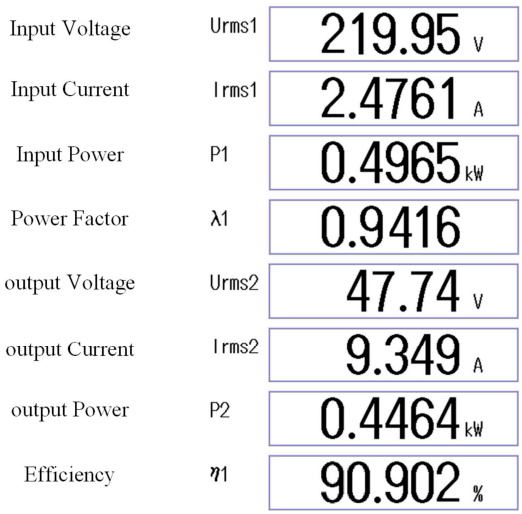
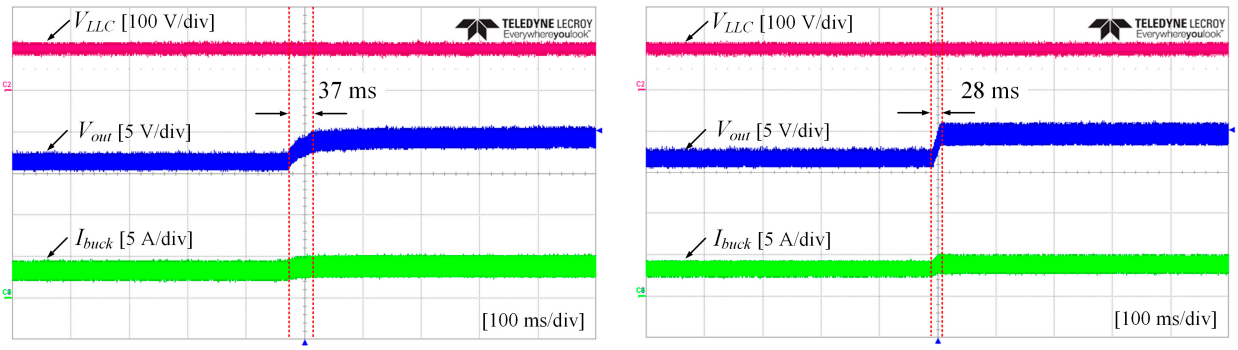


Figure 16. Experimental results of power factor and efficiency analysis in the PMD battery charger.

Figure 17 presents the experimental results of transient state responses of the battery charger, comparing the PI controller and the proposed RBFLC method. The V_{LLC} is controlled to 100 V, and the V^*_{out} is changed from 16 V to 20 V. Figure 17a presents experimental results using the PI controller, with V_{out} to reach V^*_{out} in 37 ms. Adjusting the gain of the PI controller can improve responsiveness, which may cause overshoot. Figure 17b presents experimental results using the RBFLC method, with V_{out} to reach V^*_{out} in 28 ms. Compared to the PI controller, the proposed RBFLC method improves responsiveness by approximately 24.32%.

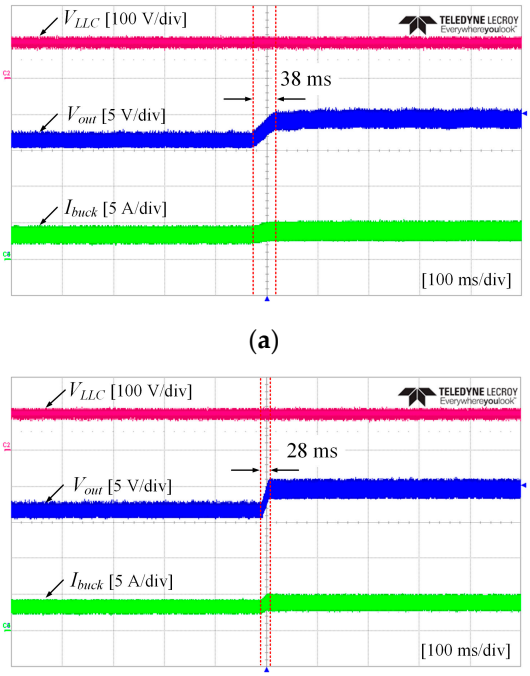


(**a**) (**b**)

Figure 17. Experimental results of transient state responses: (**a**) PI controller; (**b**) proposed RBFLC.

Figure 18 presents the experimental results of the proposed RBFLC method for different values of η. Increasing the value of η improves responsiveness. Figure 18a presents the experimental results when η is set to 0.01, with V_{out} to reach V^*_{out} in 38 ms. Figure 18b presents the experimental results when η is set to 0.05, with V_{out} to reach V^*_{out} in 28 ms. Figure 18c presents the experimental results when η is set to 0.1, with V_{out} to reach V^*_{out} in 24 ms. Considering the change of I^*_{buck} during one sampling period, setting η over 0.1 increases the impact of the compensated ΔI^*_{buck}; therefore, an η value of 0.05 is suitable for the proposed RBFLC method.

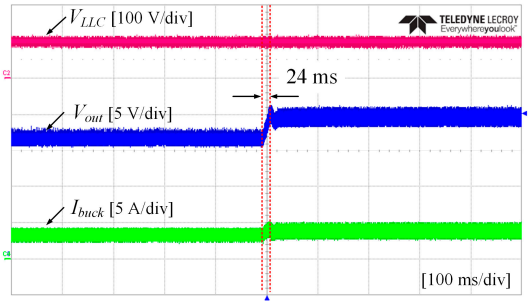
Table 3 shows the comparison of performance between the PI controller and the proposed RBFLC. The results demonstrate improved response performance under both simulation and experimental conditions.



(**a**)

(**b**)

Figure 18. *Cont.*



(**c**)

Figure 18. Experiment results of the proposed RBFLC method for different values of η: (**a**) η is 0.01; (**b**) η is 0.05; (**c**) η is 0.1.

Table 3. Comparison of performance between PI and proposed RBFLC.

Case	Controller	Rise Time	Steady State Error	Improvement
Simulation	PI	34.36 ms	0.04 mV	-
Simulation	RBFLC	26.82 ms	0.02 mV	21.9%
Experiment	PI	37 ms	-	-
Experiment	RBFLC	28 ms	-	24.3%

6. Conclusions

In this paper, the RBFLC method is proposed to improve the transient response of the battery charger for PMD. In general, the PI controller requires increasing the gain to enhance the transient response, which can cause oscillations and instability. In addition, the conventional FLC method using a single input variable provides strong robustness against disturbances and reduces oscillations compared with the PI controller. However, the control accuracy of the conventional FLC method is limited due to a single input variable. Therefore, in this paper, a proposed RBFLC using two input variables with triangular membership functions and the fuzzy rule-based table consisting of 49 rules can improve the transient response of the PMD battery charger compared with the PI controller. The proposed RBFLC method was verified through simulation and experiments.

Author Contributions: Conceptualization, software, simulation validation, writing—original draft preparation, and visualization, G.Y.; experimental validation, Y.B. All authors have read and agreed to the published version of the manuscript.

Funding: This research was supported by the National Research Foundation of Korea (NRF) grant funded by the Korea government (MSIT) (No. RS-2025-23323395).

Data Availability Statement: The original contributions presented in this study are included in the article. Further inquiries can be directed to the corresponding author.

Conflicts of Interest: The authors declare no conflicts of interest.

References

1. Lim, S.-K.; Lee, H.-S.; Cha, H.-R.; Park, S.-J. Multi-level DC/DC converter for E-mobility charging stations. *IEEE Access* **2020**, *8*, 48774–48783. [CrossRef]
2. Marsic, V.; Igic, P.; Pandey, V.; Zhou, W.; Faramehr, S. Experimental low-cost magnetic scanning for non-destructive testing with hall sensors: Determining material's thickness. *IEEE Access* **2025**, *13*, 65105–65120. [CrossRef]
3. Vasiladiotis, M.; Rufer, A. A modular multiport power electronic transformer with integrated split battery energy storage for versatile ultra-fast EV charging stations. *IEEE Trans. Ind. Electron.* **2015**, *62*, 3213–3222. [CrossRef]
4. Nakajima, S. Evaluation of the mobility performance of a personal mobility vehicle for steps. *IEEE Access* **2017**, *5*, 9748–9756. [CrossRef]

5. Moon, G.; Bak, Y. Dynamic characteristic improvement of battery charger for PMDs using a model predictive control. *IEEE Access* **2024**, *12*, 25835–25843. [CrossRef]
6. Choi, J.; Bak, Y. Chattering reduction using improved switching functions in the SMC method for battery chargers of PMDs. *IEEE Access* **2024**, *12*, 182663–182672. [CrossRef]
7. Kim, G.; Bak, Y. Improved sliding mode control for performance enhancement of PMD battery charger using fuzzy logic control. *IEEE Access* **2025**, *13*, 2080–2088. [CrossRef]
8. Nguyen, H.V.; To, D.-D.; Lee, D.-C. Onboard battery chargers for plug-in electric vehicles with dual functional circuit for low-voltage battery charging and active power decoupling. *IEEE Access* **2018**, *6*, 70212–70222. [CrossRef]
9. Shafiei, N.; Ordonez, M.; Craciun, M.; Botting, C.; Edington, M. Burst mode elimination in high-power LLC resonant battery charger for electric vehicles. *IEEE Trans. Power Electron.* **2016**, *31*, 1173–1188. [CrossRef]
10. Karneddi, H.; Ronanki, D. Universal bridgeless nonisolated battery charger with wide-output voltage range. *IEEE Trans. Power Electron.* **2023**, *38*, 2816–2820. [CrossRef]
11. Metwly, M.Y.; Abdel-Majeed, M.S.; Abdel-Khalik, A.S.; Hamdy, R.A.; Hamad, M.S.; Ahmed, S. A review of integrated on-board EV battery chargers: Advanced topologies, recent developments and optimal selection of FSCW slot/pole combination. *IEEE Access* **2020**, *8*, 85216–85242. [CrossRef]
12. Baek, J.; Kim, J.-K.; Lee, J.-B.; Park, M.-H.; Moon, G.-W. A new standby structure integrated with boost PFC converter for server power supply. *IEEE Trans. Ind. Electron.* **2019**, *34*, 5283–5293. [CrossRef]
13. Chen, H.-C.; Lan, Y.-C. Unequal duty-ratio feedforward control to extend balanced-currents input voltage range for series-capacitor-based boost PFC converter. *IEEE Trans. Ind. Electron.* **2023**, *70*, 4289–4292. [CrossRef]
14. Jia, P.; Liu, M. A wide range LLC resonant converter realized by an adjustable turns ratio transformer. *IEEE Trans. Power Electron.* **2025**, *40*, 10396–10401. [CrossRef]
15. Pacheco, L.F.; Nascimento, K.C.M.; Barbi, I. Isolated AC/AC converter with LLC resonant converter high-frequency link and four-quadrant switches in the output stage. *IEEE Access* **2020**, *8*, 213104–213114. [CrossRef]
16. Kakkar, S.; Matiy, T.; Ahuja, R.K.; Walde, P.; Saket, R.K.; Khan, B. Design and control of grid-connected PWM rectifiers by optimizing fractional order PI controller using water cycle algorithm. *IEEE Access* **2021**, *9*, 125941–125954. [CrossRef]
17. Sarsembayev, B.; Suleimenov, K.; Do, T.D. High order disturbance observer based PI–PI control system with tracking anti-windup technique for improvement of transient performance of PMSM. *IEEE Access* **2021**, *9*, 66323–66334. [CrossRef]
18. Fkirin, M.A.; Khira, M.A.-E. Enhanced antenna positioning control system using adapted DC servo motor and fuzzy-PI controller. *IEEE Access* **2023**, *11*, 102661–102668. [CrossRef]
19. Yaniv, O.; Mollov, S. Synthesizing all filtered proportional–integral and PID controllers satisfying gain, phase, and sensitivity specifications. *IEEE Trans. Ind. Electron.* **2023**, *70*, 2939–2947. [CrossRef]
20. Xie, T.; Gong, Z. A hesitant soft fuzzy rough set and its applications. *IEEE Access* **2019**, *7*, 167766–167783. [CrossRef]
21. Mahmood, T.; Ali, Z.; Gumaei, A. Interdependency of complex fuzzy neighborhood operators and derived complex fuzzy coverings. *IEEE Access* **2021**, *9*, 73506–73521. [CrossRef]
22. Jara, P.; Merino, L.; Navarro, G.; Santos, E. On gradual sets, hesitant fuzzy sets, and representation theorems. *IEEE Access* **2024**, *12*, 111158–111168. [CrossRef]
23. Saeed, M.M.; Ibrahim, H.Z. n,m-th power root fuzzy set and its applications to topology and decision-making. *IEEE Access* **2022**, *10*, 97677–97691. [CrossRef]
24. Mei, W. Formalization of fuzzy control in possibility theory via rule extraction. *IEEE Access* **2019**, *7*, 90115–90124. [CrossRef]
25. Zheng, J.; Du, W.; Nascu, I.; Zhu, Y.; Zhong, W. An interval type-2 fuzzy controller based on data-driven parameters extraction for cement calciner process. *IEEE Access* **2020**, *8*, 61775–61789. [CrossRef]
26. Sun, Z.; Bi, Y.; Zhao, X.; Sun, Z.; Ying, C.; Tan, S. Type-2 fuzzy sliding mode anti-swing controller design and optimization for overhead crane. *IEEE Access* **2018**, *6*, 51931–51938. [CrossRef]
27. Jia, K.; Lin, S.; Du, Y.; Zou, C.; Lu, M. Research on route tracking controller of quadrotor UAV based on fuzzy logic and RBF neural network. *IEEE Access* **2023**, *11*, 111433–111447. [CrossRef]
28. Karbasi, S.; Ebrahimi, J.; Hajian, A.M. Enhanced fuzzy logic controller design for alternate arm converter in short and extended overlap modes. *IEEE Access* **2025**, *13*, 172704–172716. [CrossRef]
29. Valdivia, V.; Barrado, A.; Lázaro, A.; Zumel, P.; Raga, C.; Fernández, C. Simple modeling and identification procedures for "black-box" behavioral modeling of power converters based on transient response analysis. *IEEE Trans. Power Electron.* **2009**, *24*, 2776–2790. [CrossRef]

Disclaimer/Publisher's Note: The statements, opinions and data contained in all publications are solely those of the individual author(s) and contributor(s) and not of MDPI and/or the editor(s). MDPI and/or the editor(s) disclaim responsibility for any injury to people or property resulting from any ideas, methods, instructions or products referred to in the content.